Structural Engineering and Mechanics, *Vol. 57, No. 6 (2016) 1085-1105*
DOI: http://dx.doi.org/10.12989/sem.2016.57.6.1085

Flat-bottomed design philosophy of *Y*-typed bifurcations in hydropower stations

Yang Wang[1a], Chang-zheng Shi[*1], He-gao Wu[1b], Qi-ling Zhang[2] and Kai Su[1]

[1]*State Key Laboratory of Water Resources and Hydropower Engineering Science, Wuhan University, Wuhan, Hubei 430072, China*
[2]*Changjiang River Scientific Research Institute, Wuhan, Hubei 430010, China*

(Received March 12, 2015, Revised January 29, 2016, Accepted February 4, 2016)

Abstract. The drainage problem in bifurcations causes pecuniary losses when hydropower stations are undergoing periodic overhaul. A new design philosophy for *Y*-typed bifurcations that are flat-bottomed is proposed. The bottoms of all pipe sections are located at the same level, making drainage due to gravity possible and shortening the draining time. All fundamental curves were determined, and contrastive analysis with a crescent-rib reinforced bifurcation in an actual project was conducted. Feasibility demonstrations were researched including structural characteristics based on finite element modeling and hydraulic characteristics based on computational fluid dynamics. The new bifurcation provided a well-balanced shape and reasonable stress state. It did not worsen the flow characteristics, and the head loss was considered acceptable. The proposed *Y*-typed bifurcation was shown to be suitable for pumped storage power stations.

Keywords: hydropower; bifurcation; flat-bottomed; design philosophy; finite element modeling; computational fluid dynamics

1. Introduction

Hydropower is not only a renewable and sustainable energy source, but also offers flexibility and large-scale energy storage. It makes it possible to improve the stability of power grids, and support the deployment of other intermittent renewable energy sources such as wind and solar power. As a result, pumped hydro energy storage plants (PHESs) are commonly recognized as one of the most cost-efficient energy technologies currently available (Ardizzon 2014, Nazari 2010).

Penstock functions often involve branching the tunnel or penstock into two or more penstocks for multiple hydroelectric power turbines or discharge outlets. Such branches are commonly referred to as bifurcations, as shown in Fig. 1. They require special designs that are unique to individual projects (American Society of Civil Engineers (ASCE) 2012). Bifurcations are usually employed when two or more hydro-generators are supplied by one penstock, and are important parts of the water diversion system.

∗Corresponding author, Ph.D., E-mail: scz4@163.com
[a]Ph.D., E-mail: oceans@whu.edu.cn
[b]Professor, E-mail: wbf1988@vip.sina.com

http://www.techno-press.org/?journal=sem&subpage=8 ISSN: 1225-4568 (Print), 1598-6217 (Online)

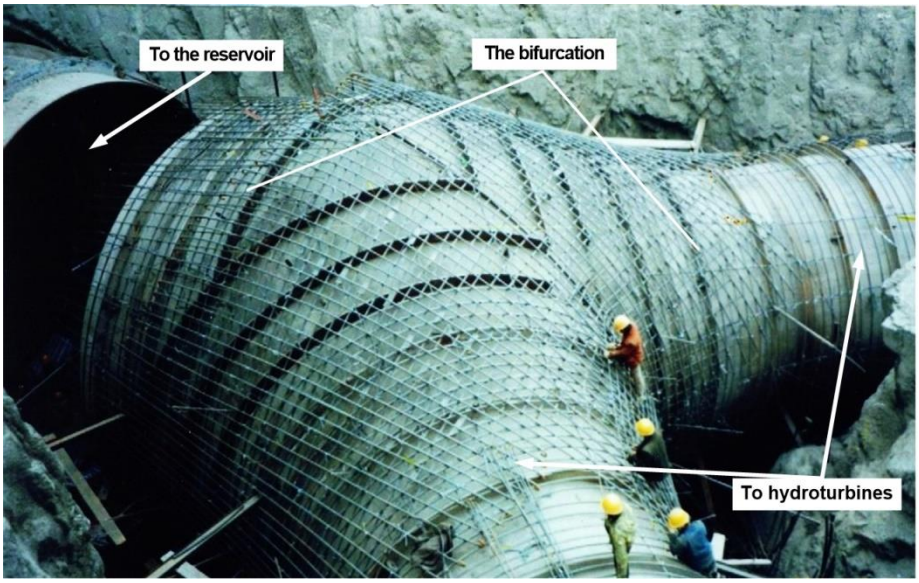

Fig. 1 The bifurcation of hydropower stations

In general, bifurcations in hydropower stations often withstand high internal water pressures (the magnitude of the water head often exceeding 100 m), and the dimensions are usually considerable (inside diameter up to 5 m). Meanwhile, the hoop action in the pipes is interrupted in the bifurcation, with extremely large unbalanced forces. Pipe reinforcements or stiffeners are typically required as additional supports for the steel shells (ASCE 2012).

Bifurcations may be reinforced with a simple curved plate designed to meet the requirements of the American Society of Mechanical Engineers for the welt bifurcation. For branch outlets that intersect in this manner, three or four exterior horseshoe girders may be used, such as the reinforced girders bifurcation (RGB). For wyes used in penstocks designed for reducing the size of girders, an internal horseshoe girder, sometimes called a rib, may be used, such as the crescent-ribbed bifurcation (CRB). This design is a common variation of the spherical header incorporating a conical shape, where the knuckle transitions between the main pipe and branch pipes (ASCE 2012). These three bifurcations are widely used, as shown in Fig. 2.

However, there is a universal problem in the bifurcations mentioned above: the drainage problem. It is essential to conduct periodic overhaul and corrosion protection of the metal structures used in hydropower stations. When the water in the diversion system is drained, a ponding in the bottom of the bifurcations is generated, as shown in Fig. 2. In general, we have dealt with this problem in two ways: by drawing water with pumps, or using special drainage systems through a hole in the bottom of the bifurcation.

Unfortunately, both have disadvantages. Drawing ponding using pumps is an inefficient measure because of the low pumping speed and time-consuming transportation of pumps. For example, in the bifurcation of Liyang PHES in China, the diameter of the main pipe is 8.5 m and the maximum depth of the ponding is 2 m. The volume is 18% of the main pipe volume, and the transportation of the pumping equipment and the drainage takes an additional 8 h during maintenance. The direct pecuniary loss has reached US$ 200,000 on account of the delays in engine production each time. Periodic overhaul is a repeated and ongoing measure, so this

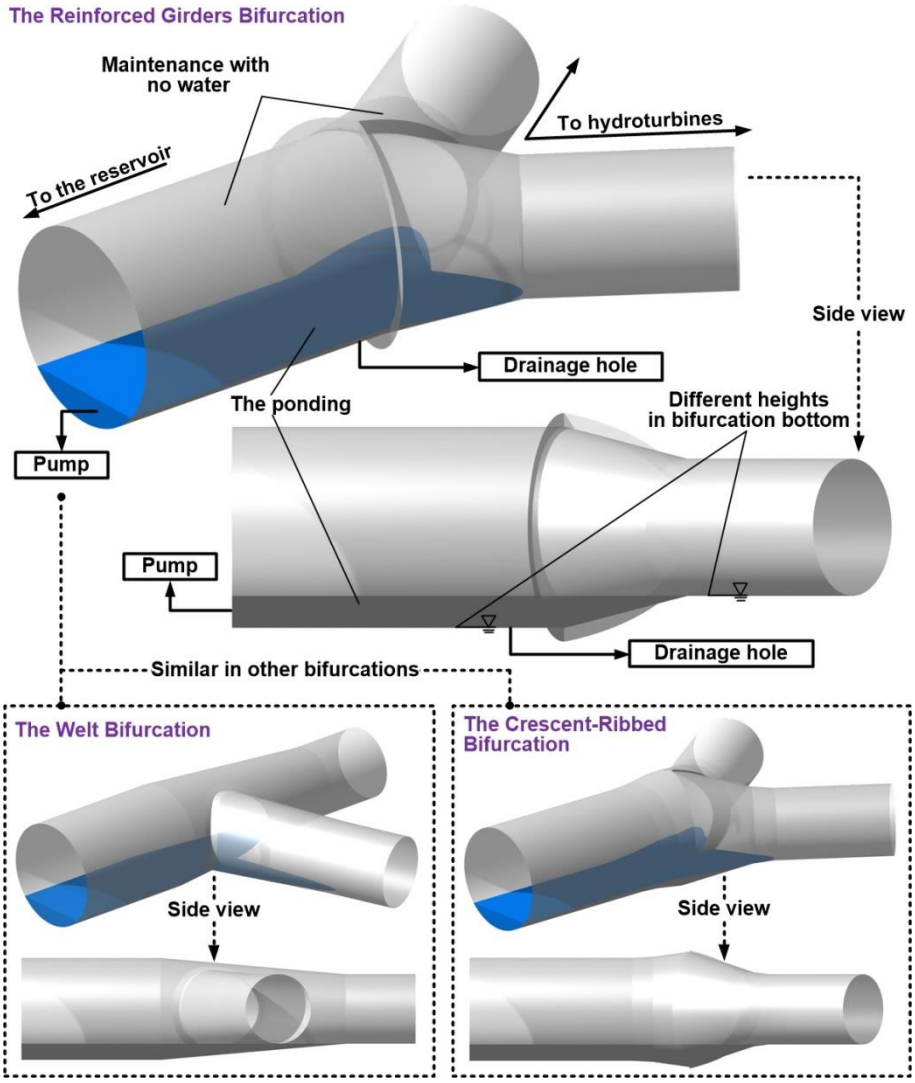

Fig. 2 Schematic of the drainage problem in hydropower bifurcations

pecuniary loss always occurs in the operation of hydropower stations. The second approach, making a hole in the bottom of the bifurcation, has not proved to be an effective solution either. The drainage systems are easily jammed because they suffer from the combination of corrosion and silt, which reduces drainage efficiency. The bifurcations in PHESs are generally made of high-tensile steel material. Making holes in steel shells, which can result in severe stress concentration, is not permitted (Storozhuk 2012a, b). Consequently, there are no efficient solutions to this drainage problem in hydropower bifurcations.

A better way of solving this problem is to modify the design shape rather than using a supplementary drainage facility. The axes of all sections are at the same level in conventional bifurcations, while the bottoms are not, which is the main cause of ponding. Therefore, we attempt to make and locate the bottoms of all pipe sections at the same level. This makes drainage due to

gravity possible, and there is no need for a draining facility or a special drainage system during the maintenance of penstocks. However, as mentioned above, the unbalanced forces of hydropower bifurcations are very large, so it is necessary to demonstrate the feasibility of the new bifurcation.

Considerable research on bifurcations has been performed because they are widely used in water distribution systems, sewage systems, and so on. Two fundamental shapes, the *T*- and *Y*-shaped junctions, are typical models, which have been widely researched experimentally and through numerical simulations.

For structural characteristics, approximate analytical approaches for the plastic limit load of T-junctions, using the relationship of the internal forces between the main and branch pipes around the intersection line, have been presented by Xuan (2005, 2006), Kim (2006, 2008), Lee (2009, 2012). Other research has focused on pressure and bending moments, and dissimilar material joints, such as the work of Xuan (2003, 2004), Hafiz (2012), Myeong (2012), Ure (2013), Papatheocharis (2013). Designs and calculations of the bifurcations in hydroelectric stations have been performed for early conventional bifurcations, for example, the work of German (1998). It shows that finite element modeling (FEM) is a mature and accurate method for simulating such models. From this we obtain insight into the turning points and intersection lines that are important for determining internal pressure.

For the hydraulic characteristics, energy loss is a major issue that has been the subject of research over preceding decades. Pérez-García (2006, 2009, 2010), Gan (2000), Tang (2009), among others, showed energy loss results that can be obtained using loss coefficients for both *T*- and *Y*-typed bifurcations. Computational fluid dynamics (CFD) has proved to be an effective means of simulation. For example, Jeong (2014) compared the effects on technical variances of CFD software focusing on the accuracy of the results and the flow patterns. Bifurcation of other shapes has also been studied, such as mixing at cross-junctions in water distribution systems by Romero-Gomez (2008) (numerical study) and Austin (2008) (experimental study), and dividing single-phase fluids on symmetric bifurcations of flow channels by Liu (2013). They showed that the streamlines bent heavily in the bifurcation process and energy loss was greater than in the straight parts of the flow path.

However, in most research, the bifurcation was performed on conventional dimensions with diameters of less than 1 m. Different from these duct junctions, the dimensions of this new proposed bifurcation for hydropower stations are usually very large (ASCE 2012). The flow in bifurcations usually has a high velocity and large Reynolds number (2010), and the intersection part was cone-shaped rather than cylindrical in most of the above research. Furthermore, the proposed new *Y*-typed flat-bottomed bifurcation has not been applied in engineering, and there are no research publications on it.

Consequently, numerical simulations and analyses on bifurcations with a high head of water and a large diameter are required, especially for this new shape. We thus performed feasibility demonstrations on both the structural and the hydraulic characteristics to check whether the stress in this new bifurcation is less than the corresponding allowable local membrane stress, whether flow separation between flow streamlines and the wall occurs, or whether large head losses develop.

The structure of this paper is as follows: Section 2 presents the design philosophy of this new bifurcation including its design, the definition of shape parameters, coordinate systems, and geometric equations of each fundamental curve. In Section 3, feasibility demonstrations are performed on the above design philosophy, including discussions on structural characteristics based on FEM, hydraulic characteristics based on CFD, and economic efficiency. Conclusions are

drawn in Section 4.

2. Design philosophy

2.1 Design of the bifurcation

The drainage problem described above is mainly caused by the different levels of the bifurcation bottoms. As a consequence, the most direct method is to ensure the pipe bottoms are maintained at a constant level. We make a shape transformation based on the RGB, a bifurcation that is widely used and considered reliable. A schematic of the design idea is shown in Fig. 3. This new type of *Y*-typed bifurcation is named the flat-bottomed bifurcation (FBB) in this paper.

The FBB comprises two parts: the pipe shells and the reinforced girders, as shown in Fig. 4. Pipe shells consist of the main pipe, cone pipe, and branch pipe, and the reinforced girders consist of the waist and *U*-shaped girders.

For the pipe shells, the bottoms of all of the pipe segments lie at the same elevation because of the tilt of the pipe axis. At the same time, the intersecting curve of the main and cone pipes is a plane curve because of their common tangent spheres. Similarly, the intersecting curve of the cone pipe and the branch pipe is a plane curve. This design is derived from the basic pipe shape of the RGB, which is a mature application judging from existing engineering, such as the GIBE 3rd hydroelectric project in Ethiopia and the Tarbela 4th Extension Project in Pakistan. The FBB retains the major advantages of the RGB, including easy interfacing and installing, and the bearing capacity.

For reinforced girders, the waist reinforced girders and *U*-shaped girder are retained, as in the RGB. The waist reinforced girders are set at the intersecting curve of the main pipe and the cone pipe, and the *U*-shaped reinforced girder is set at the intersecting curve of the two cone pipes. This is because the cross-section of two cone pipes is larger than other pipe junctions in bifurcations, and the unbalanced force here is larger than in other conventional systems and needs to be restrained. However, different from the RGB, a rib is set inside the bifurcation as part of the *U*-shaped reinforced girder. This design was inspired from the CRB, which was widely used in existing engineering practice in recent decades, such as the CCS Project in Ecuador and the NAM

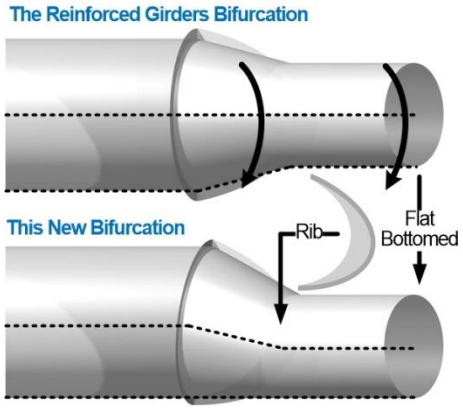

Fig. 3 Design concept to solve the drainage problem: a flat-bottomed bifurcation

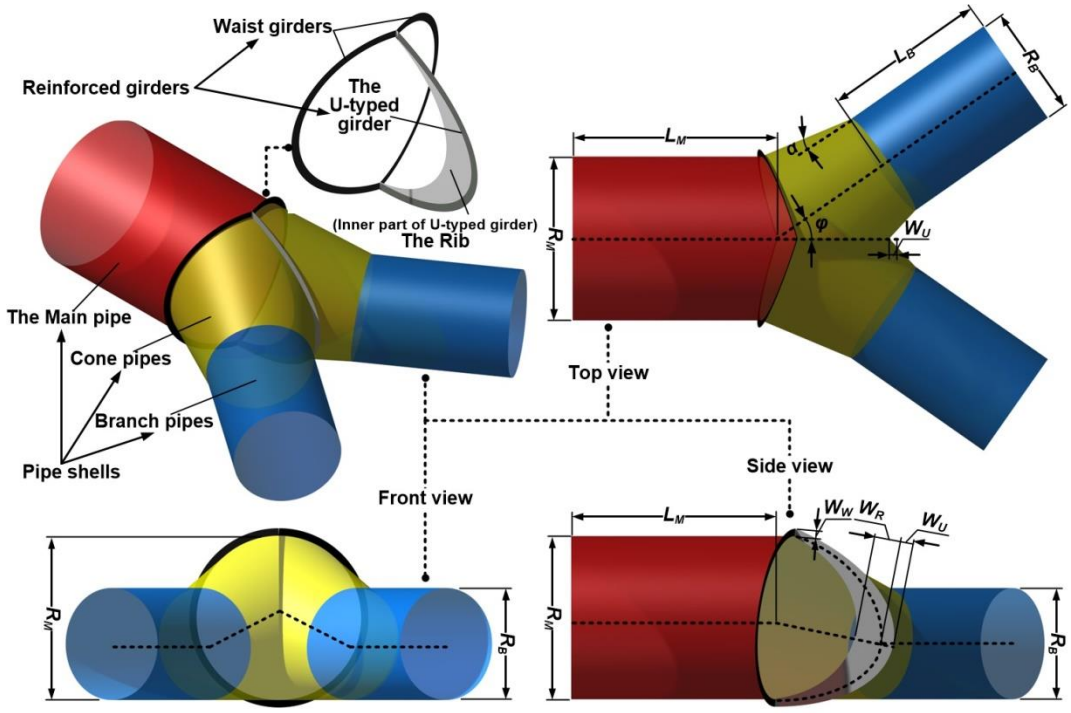

Fig. 4 FBB and definitions of shape parameters

OU 6th project in Lao People's Democratic Republic. It was able to consolidate the *U*-shaped reinforced girder effectively, and decrease the external extension width of the reinforced girders. The rib is parallel to the flow direction in the main pipe, so the small disturbances of flow characteristics are generated.

2.2 Definition of shape parameters

In this study, we selected nine basic shape parameters, namely the horizontal projection angle of the bifurcation (φ), radius of the main pipe (R_M), radius of the branch pipe (R_B), taper apex angle of the cone pipe (α), axis length of the main pipe (L_M), axis length of the branch pipe (L_B), width of the waist reinforced girders (W_W), width of the *U*-shaped extension reinforced girder (W_U), and maximum width of the rib (W_R). In this way, the bifurcation shape is uniquely determined by these parameters. The basic shape parameters above are shown in Fig. 4.

2.3 Definitions of coordinate systems

To obtain a realizable design philosophy of the *FBB*, we needed to establish geometric equations for each profile curve. Thus, a rectangular Cartesian coordinate system named *OXYZ* was established, which was the datum coordinate system (CSYS) in this study (Thomas 1988, Yamaguchi 1988). In *OXYZ*, the *XOY* plane was taken to be the horizontal plane, and the *Z*-axis set vertically upward. The origin was located at the intersection point of the main pipe axis and the cone pipe axes, which was also the center of the common tangent (as shown in Fig. 5).

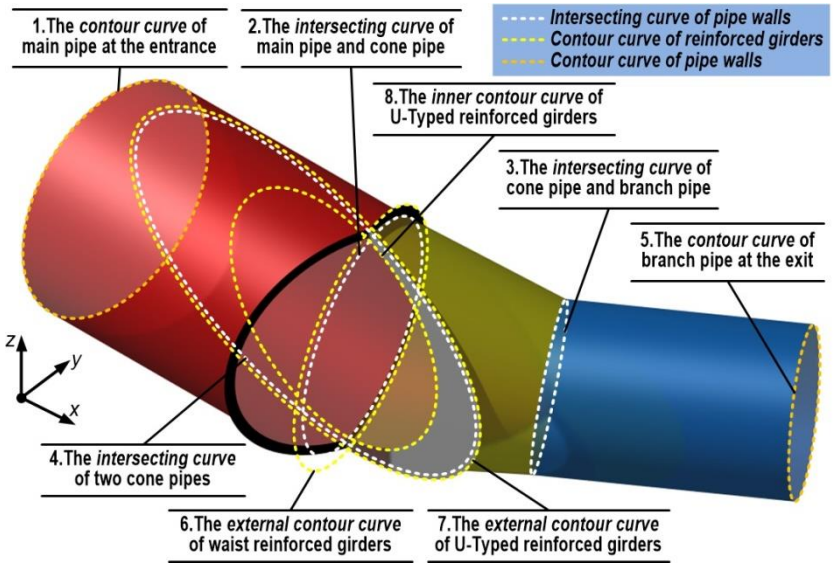

Fig. 5 Location and type of each fundamental curve

In the *FBB*, the axes of the main pipe, the cone pipe, and the branch pipe were not in a horizontal plane, and intersecting curves between each of the two pipes were complex. Because all of the intersecting curves were conic curves, each intersecting curve was in a plane. However, these curves were not symmetrical about the *XOY* plane in *OXYZ*. As a consequence, we defined three local coordinate systems, named $O_1X_1Y_1Z_1$, $O_2X_2Y_2Z_2$, and $O_3X_3Y_3Z_3$. Geometric equations of the intersecting curves are expressed more concisely under these local coordinate systems (Seppälä 2012). Each local coordinate system can be transformed to *CSYS*.

2.4 Geometric equations

It can be seen from the analysis above that the bifurcation is created when all of the curves are determined. In this study, some fundamental curves are defined including profile curves and intersecting curves. The bifurcation can be uniquely shaped by these eight fundamental curves (as shown in Fig. 5).

To express the geometric equations of the fundamental curves more concisely, we define six interim parameters: λ, γ, β, μ, m, and δ. All of the equations are expressed in terms of the parameter equations, where the range of the parameter is $\theta \in [0,2\pi]$ (Thomas 1988, Yamaguchi 1988). The geometric equations and the definition of interim parameters are presented in Eqs. (1)-(18) below.

2.4.1 Contour curve of the main pipe at the entrance

The main pipe is a cylinder in *OXYZ*, so the contour curve of the main pipe is a circle at the entrance. The geometric equations can be expressed as Eq. (1)

$$\begin{cases} x = -L_M \\ y = R_M \cos\theta \\ z = R_M \sin\theta \end{cases}. \tag{1}$$

2.4.2 Intersecting curve of the main and cone pipes

The main pipe and the cone pipe have a common tangent in the FBB. As a result, the intersecting curve of these two pipes is an ellipse. The geometric equations can be expressed as Eq. (2)

$$\begin{cases} x = \dfrac{R_M \sin\alpha - R_M \sin\gamma\cos\theta}{\cos\alpha + \cos\gamma} \\ y = R_M \cos(\theta - \lambda) \\ z = R_M \sin(\theta - \lambda) \end{cases}, \tag{2}$$

where the interim parameters λ and γ are defined in Eqs. (3)-(4).

$$\sin^2\lambda = \sin^2\alpha + \sin^2\varphi\cos^2\alpha, \tag{3}$$

$$\sin\gamma = \frac{\sin\alpha}{\sin\lambda}. \tag{4}$$

2.4.3 Intersecting curve of the cone and branch pipes

The cone pipe and branch pipe also have a common tangent similar to the intersecting curve of the main pipe and cone pipe as shown in Eq. (4). The geometric equations can be expressed as Eq. (5)

$$\begin{cases} x = \left(\dfrac{R_B\sin\alpha + R_B\sin\alpha\sin\theta}{2\cos\alpha} + \dfrac{R_M - R_B}{\tan\alpha}\right)\cos\varphi - R_B\sin\varphi\cos\theta \\ y = \left(\dfrac{R_B\sin\alpha + R_B\sin\alpha\sin\theta}{2\cos\alpha} + \dfrac{R_M - R_B}{\tan\alpha}\right)\sin\varphi + R_B\cos\varphi\cos\theta \\ z = R_B\sin\theta - R_M + R_B \end{cases}. \tag{5}$$

2.4.4 Intersecting curve of the two cone pipes

The two cone pipes are symmetrical about the *XOZ* plane in *OXYZ*, and the intersecting curve of these two pipes is an ellipse in the *XOZ* plane. However, the axes of the ellipse are not parallel to the *x*-axis, so we express the geometric equations in terms of $O_1X_1Y_1Z_1$ for simplicity. The geometric equations can be expressed as Eq. (6)

$$\begin{cases} x_1 = \dfrac{m\cos\alpha\sin\alpha}{\cos^2\alpha - \sin^2\beta}\cos\theta - \dfrac{m\cos\beta\sin\beta}{\cos^2\alpha - \sin^2\beta} \\ y_1 = 0 \\ z_1 = \dfrac{m\sin\alpha}{\sqrt{\cos^2\alpha - \sin^2\beta}}\sin\theta \end{cases}, \tag{6}$$

where the interim parameters β, μ, and m are defined in Eqs. (7)-(9)

$$\cos\beta = \sin\varphi\cos\alpha\,, \tag{7}$$

$$\tan\mu = \frac{\tan\alpha}{\cos\varphi}, \tag{8}$$

$$m = \frac{R_M \sin\varphi}{\tan\alpha}\,. \tag{9}$$

Here the coordinates in $O_1X_1Y_1Z_1$ need be transformed to those in *OXYZ*. The coordinate transformation equation is shown in Eq. (10)

$$\begin{bmatrix} x \\ y \\ z \end{bmatrix} = \begin{bmatrix} \cos\mu & 0 & \sin\mu \\ 0 & 1 & 0 \\ -\sin\mu & 0 & \cos\mu \end{bmatrix} \begin{bmatrix} x_1 \\ y_1 \\ z_1 \end{bmatrix} + \begin{bmatrix} R_M/\tan\mu \\ 0 \\ -R_M \end{bmatrix}. \tag{10}$$

2.4.5 Contour curve of the branch pipe at the exit

The branch pipe is a cylinder, but the contour curve at the exit is not parallel to the *YOZ* plane in *OXYZ*. Geometric equations should be transformed to *CSYS* as shown in Eq. (11)

$$\begin{cases} x = \left(L_B + \dfrac{R_M - R_B}{\tan\alpha}\right)\cos\varphi - R_B\sin\varphi\cos\theta \\ y = \left(L_B + \dfrac{R_M - R_B}{\tan\alpha}\right)\sin\varphi + R_B\cos\varphi\cos\theta\,. \\ z = R_B\sin\theta - R_M + R_B \end{cases} \tag{11}$$

2.4.6 External contour curve of the waist reinforced girders

The external contour curve of the waist reinforced girders is similar to the intersecting curve of the main and cone pipes (as shown in Eq. (2)). In fact, these two curves are in the same plane, but the former is offset outside the latter. Therefore, we express the geometric equations in terms of $O_2X_2Y_2Z_2$ for simplicity. The geometric equations can be expressed as Eq. (12)

$$\begin{cases} x_2 = 0 \\ y_2 = \left(\dfrac{R_M}{\cos\delta} + W_W\right)\cos\theta\,, \\ z_2 = \left(R_M + W_W\right)\sin\theta \end{cases} \tag{12}$$

where the interim parameter δ is defined in Eq. (13).

$$\tan\delta = \frac{\sin\gamma}{\cos\alpha + \cos\gamma}\,. \tag{13}$$

Here the coordinates in $O_2X_2Y_2Z_2$ need to be transformed to those in *OXYZ*. The coordinate transformation equation is given by Eq. (14)

$$\begin{bmatrix} x \\ y \\ z \end{bmatrix} = \begin{bmatrix} \cos\delta & -\sin\delta & 0 \\ \cos\lambda\sin\delta & -\cos\lambda\cos\delta & \sin\lambda \\ -\cos\lambda\sin\delta & -\cos\lambda\cos\delta & \cos\lambda \end{bmatrix} \begin{bmatrix} x_2 \\ y_2 \\ z_2 \end{bmatrix} + \begin{bmatrix} R_M \sin\alpha\tan\delta/\sin\gamma \\ 0 \\ 0 \end{bmatrix}. \tag{14}$$

2.4.7 External contour curve of the U-shaped reinforced girders

The method of determining the geometric equations here is comparable to that for the waist reinforced girders. Thus, the external contour curve of the *U*-shaped reinforced girders is offset outside the intersecting curve of the two cone pipes. Therefore we express the geometric equations in terms of $O_1X_1Y_1Z_1$, similar to Eq. (8). The geometric equations can be expressed as Eq. (15)

$$\begin{cases} x_1 = \left(\dfrac{m\cos\alpha\sin\alpha}{\cos^2\alpha - \sin^2\beta} + W_U \right)\cos\theta - \dfrac{m\cos\beta\sin\beta}{\cos^2\alpha - \sin^2\beta} \\ y_1 = 0 \\ z_1 = \left(\dfrac{m\sin\alpha}{\sqrt{\cos^2\alpha - \sin^2\beta}} + W_U \right)\sin\theta \end{cases}. \tag{15}$$

2.4.8 Inner contour curve of the U-shaped reinforced girders

The rib is inside the bifurcation as part of the *U*-shaped reinforced girders. With reference to the commonly used *CRB*, the inner contour curve of the rib is selected as a parabola. The axis of the cone pipe is not horizontal, so the contour curve needs to be considered in two parts. It is separated by the projection of the cone pipe axis to the *XOZ* plane in *OXYZ*. Geometric equations of the upside and downside parts can be expressed respectively by Eq. (16) and Eq. (17) in $O_3X_3Y_3Z_3$

$$x_3 = \frac{R_M\left[\dfrac{\cos\mu(\sin\alpha + \sin\gamma\sin\lambda)}{\cos\alpha + \cos\gamma} - \dfrac{\sin^2\mu + 1}{\sin\mu}\right] + \dfrac{m(\sin\beta\cos\beta - \cos\alpha\sin\alpha)}{\cos^2\alpha - \sin^2\beta} + W_B}{R_M^2\left[\dfrac{\sin\mu(\sin\alpha + \sin\gamma\sin\lambda)}{\cos\alpha + \cos\gamma} - \cos\mu\right]^2} z_3^2 + \frac{m\sin\alpha\cos\alpha}{\cos^2\alpha - \sin^2\beta} - W_B \tag{16}$$

$$x_3 = \frac{\dfrac{R_M(\sin^2\mu - 1)}{\sin\mu} + \dfrac{m(\sin\beta\cos\beta - \cos\alpha\sin\alpha)}{\cos^2\alpha - \sin^2\beta} + W_B}{R_M^2\cos^2\mu} z_3^2 + \frac{m\sin\alpha\cos\alpha}{\cos^2\alpha - \sin^2\beta} - W_B. \tag{17}$$

Here the coordinates in $O_3X_3Y_3Z_3$ need to be transformed to those in *OXYZ*. The coordinate transformation equation is given by Eq. (18).

$$\begin{bmatrix} x \\ y \\ z \end{bmatrix} = \begin{bmatrix} \cos\mu & 0 & \sin\mu \\ 0 & 1 & 0 \\ -\sin\mu & 0 & \cos\mu \end{bmatrix} \begin{bmatrix} x_3 \\ y_3 \\ z_3 \end{bmatrix} + \begin{bmatrix} R_M/\tan\mu - (m\sin\alpha\cos\alpha)/(\cos^2\alpha - \sin^2\beta) \\ 0 \\ -R_M \end{bmatrix}. \tag{18}$$

Using Eqs. (1)-(18), all of the fundamental curves can be determined in *CSYS*, and the bifurcation can be shaped uniquely. Through this realizable design philosophy, we can obtain the

coordinates of each point on the bifurcation directly.

3. Feasibility demonstration

The *FBB* has not been applied in actual engineering projects. Thus there are no measured project data. We have designed a bifurcation based on the design philosophy above, and have performed contrastive analysis with the *CRB* of a *PHES* in China, which is widely used in present engineering practice since the relatively evenly distributed stress, less water head loss and good economics. The feasibility analysis was achieved using numerical simulations, including the structural characteristics based on *FEM* and hydraulic characteristics based on *CFD*.

3.1 Mathematical and computational models

3.1.1 Mathematical models

(1) Element types and real constants of the FEM

In finite element grids of the bifurcation, pipe shells were produced using the shell elements with four nodes, which ensured calculation accuracy and fine grid shapes (Dhatt 2012). Considering the relative thickness of the ribs, solid elements with eight nodes were employed in the simulations. In this study they were realized with an *FEM* solver. Pipe shells and reinforced girders were made of steel, of which the elastic modulus was assumed to be 206.0 GPa and Poisson's ratio was taken as 0.3 (ASCE 2012).

(2) Turbulence model of CFD

In the Reynolds-averaged Navier-Stokes approach (Wilcox 1993), the k-ε model is widely adopted for engineering applications on account of its reasonable computational effort, good accuracy and applicability. Taking into account the bifurcation flow characteristics and the established practice for related problems, a realizable k-ε model (Shih 1995) was adopted that could predict the expansion rate of both planar and round jets more accurately. It could provide superior performance for flows involving rotations, boundary layers under strong adverse pressure gradients, separations, and recirculation.

(3) Solver and assurance measures for computation reliability

In FEM, calculation models were performed using the commercial software ANSYS (ANSYS Inc. 2011). To decrease the effects of local stress at the restrained ends, an adequate length of the main pipe and the branch pipe was adopted. These were greater than 1.5 times the length of the maximum common tangent ball diameter, where the ball center was located in the upstream and downstream directions along the axes (Zhang 2013).

In *CFD*, the governing equations were established using the commercial software ANSYS FLUENT (ANSYS Inc. 2011). The finite volume method integrated the governing equations to construct algebraic equations that were solved using the first-order upwind and implicit scheme (Ferziger 2012). The velocity and pressure equations were coupled using the SIMPLEC algorithm (Van 1984). To ensure computation reliability, the simulations adopted certain specific treatments, such as providing sufficient cells and performing sensitivity analysis of the mesh, selecting appropriate boundary conditions, allowing a tiny iteration error, and making sure that the iteration was convergent (Cheng 2005). Some of the accuracy measures were similar to the research by

Pérez-García (2006), Liu (2013), Jeong (2014) on large eddy simulations of hydraulic characteristics in bifurcations.

Methods for the numerical simulations above were suitable for the structural and hydraulic analysis of bifurcations, and have been proved to have good precision.

3.1.2 Computational models

(1) Computational domains

The computational models were built up based on the bifurcation of a PHES in China. The radius of the main inlet pipe was 2.2 m, the radius of the branch outlet pipe 1.5 m, the bifurcation angle 65°, the internal water pressure value 1.86 MPa, and the rated discharge value 80.6 m^3/s.

Representative combined and separated flows were observed under different working conditions when one or two hydro-turbines were operating. Incompressible flow (White 2008) was assumed in the simulation analyses in this study.

(2) Boundary conditions

In FEM, the ends of the main and branch pipes were considered to be fully restrained and fixed (as shown in Fig. 5) (Dhatt 2012). The elements in contact with water were under constant internal pressure.

In CFD, we defined the boundary conditions for each inlet and outlet of the bifurcation, named Sections 1-3. Three working conditions that commonly occur in practice were considered in this study: working condition *A* had two turbines working, working condition *B* had one turbine working, and working condition *C* had two pumps working. For example, for working condition A, the main branch inlet velocity was imposed at the main pipe inlet (INLET at Section 3) and the lateral-flow ratios with pressure were imposed at the two branch outlets (OUTLET1 at Section 1 and OUTLET2 at Section 2). These three working conditions are shown in Fig. 6. At the walls, the usual nonslip conditions, adiabatic flows, and wall roughness heights were prescribed.

(3) Mesh model

In FEM, because of the relatively large pipe diameter, the generated grids were made with elements on a rather small scale. The straight and cone pipe sections were subdivided into 36 equal parts along the circumference. The thicknesses of pipe shells were optimized according to the FEM calculation results. One thinner thickness was selected on condition that the stress of steel was among the allowance. To ensure comparability of the bifurcation in practice, the thickness of the pipe shells was assumed to be 30 mm, and the thickness of all of the reinforced girders was 60 mm.

In CFD, hybrid meshes were adopted, which consisted of hexahedral cells in most of the pipes and tetrahedral cells near the rib regions. Boundary layer meshes were generated near the wall. There were approximately 4.5 million (*FBB*) and 5.4 million (*CRB*) cells in total.

Optimizations were applied according to the flow patterns and simulation experience, which eliminated the dependency of the simulation results on the mesh. Fig. 6 shows a schematic of computational models.

3.1.3 Defining stress and head loss

(1) Stress

According to the specification of ASCE (2012), the calculated stress of the steel bifurcation was satisfied by the following conditions in Eq. (19). This was based on the Von Mises yield

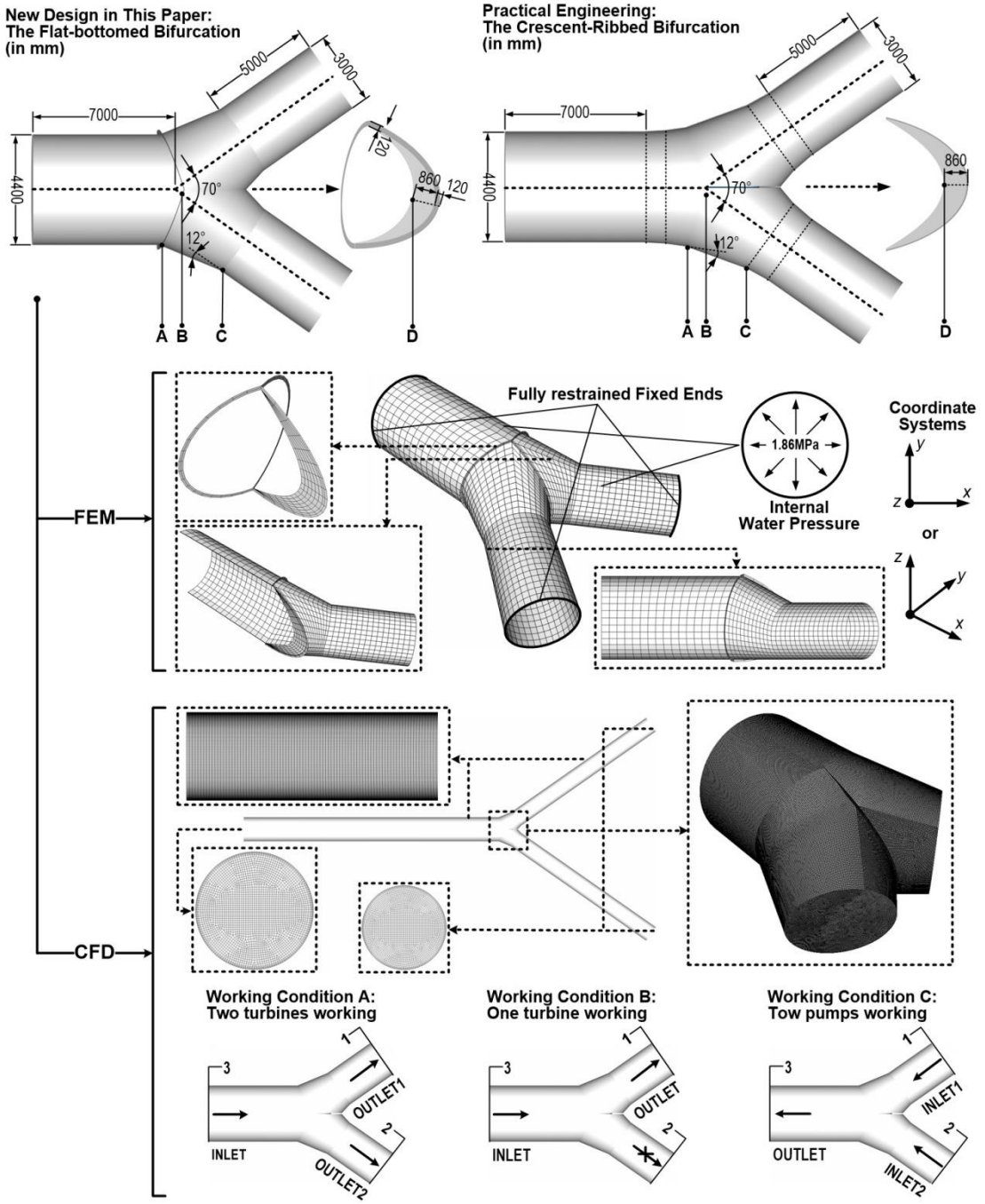

Fig. 6 Schematic of computational models including computational domains, boundary conditions, and mesh models in *FEM* and *CFD*

criterion that suggested the yielding of materials began when the second deviatoric stress invariant reached a critical value.

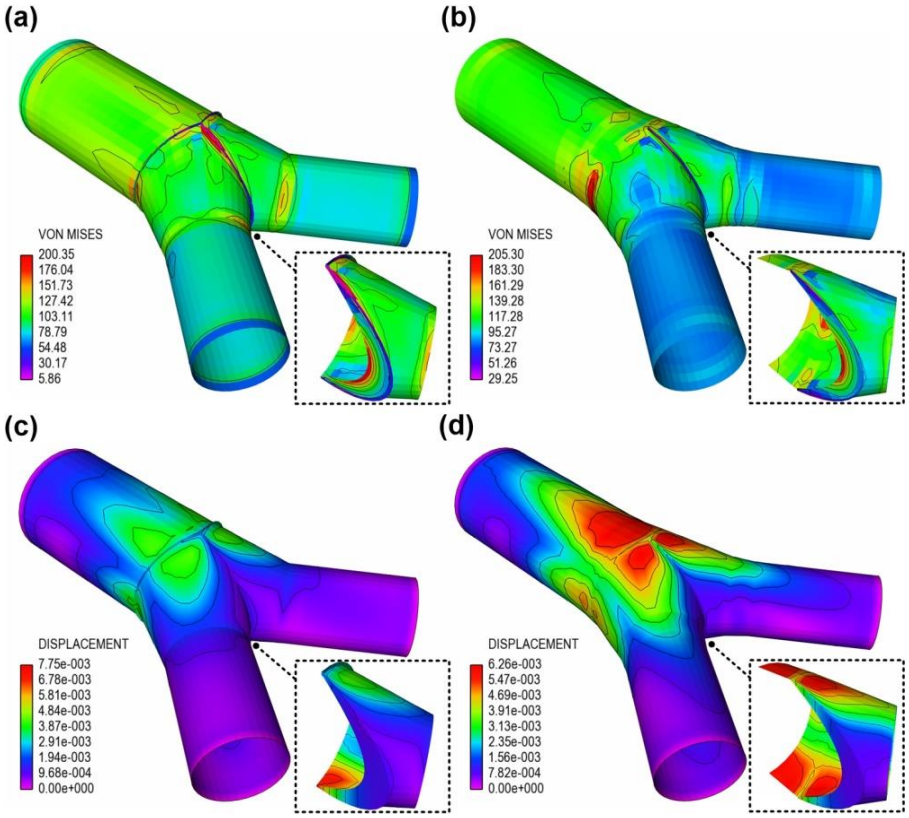

Fig. 7 Elements of Von Mises stress (in MPa) and the displacements (in m) of bifurcations: (a) and (c) the *FBB*; (b) and (d) the *CRB*

$$\sigma = \sqrt{\sigma_\theta^2 + \sigma_x^2 + \sigma_r^2 - \sigma_\theta\sigma_x - \sigma_x\sigma_r - \sigma_r\sigma_\theta + 3\left(\tau_{\theta x}^2 + \tau_{xr}^2 + \tau_{r\theta}^2\right)} \le [\sigma]. \tag{19}$$

More details on the Von Mises criterion can be found in the above-mentioned reference.

(2) Head loss

A widely used definition expresses the loss coefficient K_{ij} as a function of the reduction in stagnation (or total) pressure in Eq. (20). In this study, it is referred to as the stagnation pressure loss coefficient, as in Bassett's research (2001).

$$K_{ij} = \frac{\left(p_i + \frac{1}{2}\rho u_i^2\right) - \left(p_j + \frac{1}{2}\rho u_j^2\right)}{\frac{1}{2}\rho u_M^2}, \tag{20}$$

where subscripts i and j denote the up- and downstream branches of the junction, between which the pressure loss under consideration occurs, and subscript M denotes the main pipe, through which the entire mass flow through the junction passes. More details can be found in the above-mentioned reference.

3.2 Structural characteristics based on FEM

In accordance with the calculation results, the elements of the Von Mises stress in the pipe shells and reinforced girders as well as the displacements of the steel bifurcation are shown in Fig. 7 (with stress units in MPa and displacement units in m). Analyses of the bifurcations were performed under working condition *A*.

3.2.1 Stress and displacement distributions

To conveniently analyze the stress distributions of the two bifurcations, four key points were selected in the positions of two bifurcations, as shown in Fig. 6. These are the waist turning point of the main pipe and the cone pipe (key point *A*), the intersection point of the main pipe and two cone pipes (key point *B*), the waist turning point of the branch pipe and the cone pipe (key point *C*), and the inner lateral at the maximum cross-section (key point *D*).

We can see from Fig. 6 that the stress and displacement distributions of the *FBB* were similar to those of the *RGB*. In the pipe shells, the maximum Von Mises stress was observed at key point *A*, while in the ribs it was at key point *D*. The stress state of the *FBB* was feasible compared with the bifurcations in practice. The maximum Von Mises stress for the reinforced girders was at the top of the *U*-shaped girder near key point *B*. One interesting feature is that the maximum element Von Mises value of the *FBB* was 2.4% less than that in practice.

The maximum displacement was observed near key point *B*. Although the displacement distribution in the *FBB* was similar to that in practice, the maximum displacement was 23.8% larger than that in the latter. This was mainly because *RGB* had a geometric symmetry plane (the *XOY* plane as shown in Fig. 5), but the *FBB* had an asymmetric shape. Consequently, the displacement was asymmetric in *RG*B, but here the displacement at the bottom was clearly greater than that at the top near key point *B*.

Taken together, there were no significant stress concentration areas or clear large displacements in the *FBB*. The structural characteristics were similar to the *CRB*.

3.2.2 Peak stresses

We list the peak Von Mises stresses at the key points in the *FBB* and *CRB* found in practice, in Table 1, to identify the detailed stress distribution.

From Table 1, the Von Mises stress at key point *A* was 21.3% less than that in the *CRB* mainly because of the constraining reinforced girders. There were reinforced girders at the intersection line of the branch and cone pipes, and no transition pipes between the branch pipe and the cone pipe for the *CRB*. As a result, the peak stress at key point *C* was 5.3% greater than that found in practice, but less than the corresponding allowable local membrane stress. We note that the peak stress in the *FBB* at key point *B* was nearly as large as that in the *CRB*, which demonstrates the

Table 1 Peak Von Mises stresses at key points in the *FBB* and the *CRB*

Key points	*A*		*B*		*C*		*D*	
	The *FBB*	The *CRB*	The *FBB*	The *CRB*	The *FBB*	The *CRB*	The *FBB*	The *CRB*
Peak stress /MPa	177.491	225.511	151.304	155.229	220.929	209.191	223.979	211.734
Location	Bottom of the shell	Bottom of the shell	Top of the shell	Bottom of the shell	Top of the shell	Top of the shell	Inner lateral at the max. cross-section	

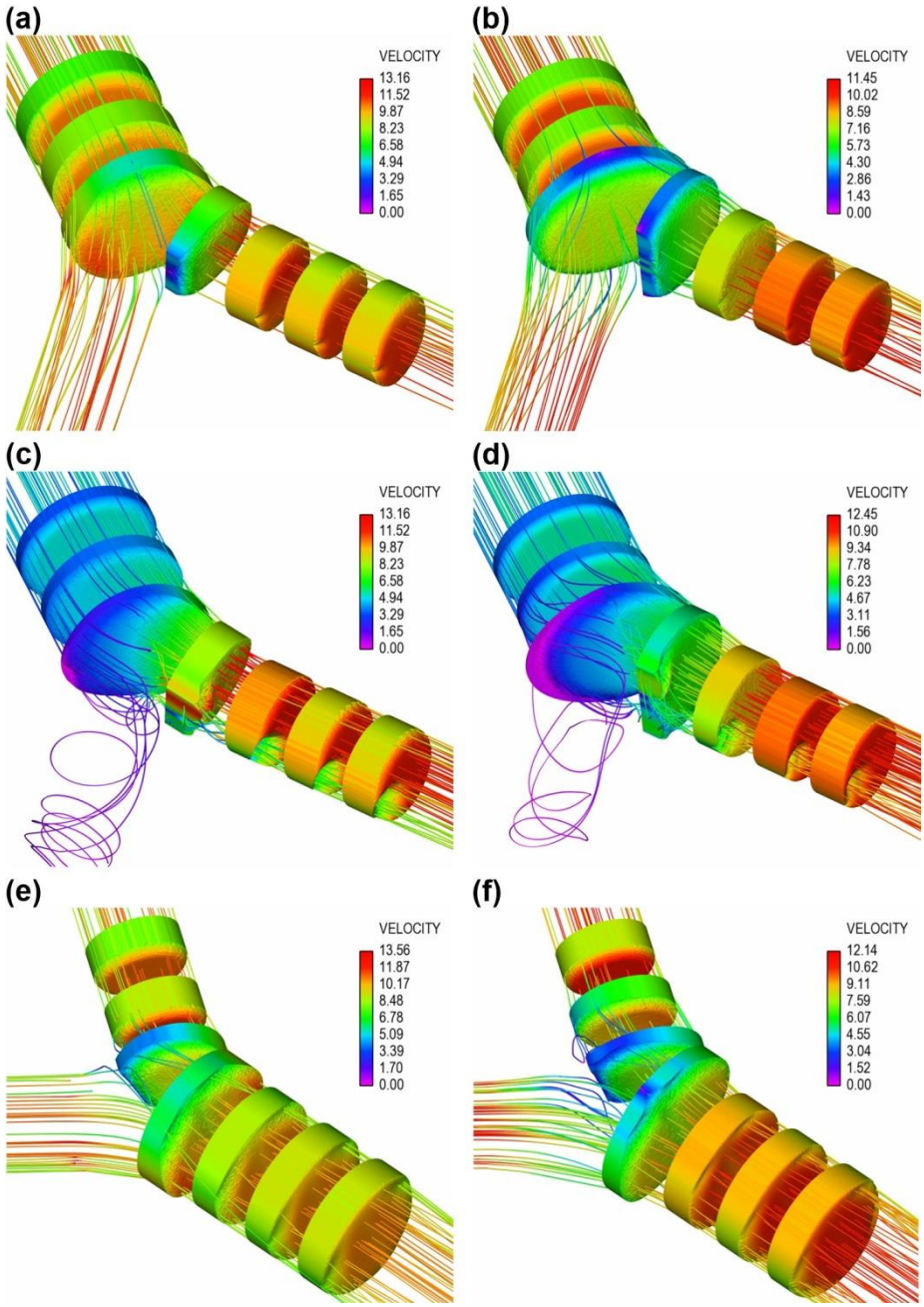

Fig. 8 Flow patterns and velocity distributions (in m/s): (a), (c), and (e) the *FBB* under working conditions *A*, *B*, and *C*; (b), (d), and (f) the *CRB* under working conditions *A*, *B*, and *C*

structural feasibility for this new shape.

Structural characteristics based on *FEM* proved that the mechanics were reasonable in the *FBB*. The majority of stresses were lower than found in practice for the same pipe thickness.

3.3 Hydraulic characteristics based on CFD

We have assessed the structural characteristics, the feasibility and the practicability of the *Y*-typed *FBB*. However, whether the change in shape of the bifurcation affects the hydraulic characteristics needs further research. Based on the practical engineering model mentioned above, the *FBB* and the *CRB* were then compared, with a focus on the hydraulic characteristics. We consider three working conditions commonly found in hydro-generator operations (*A*-*C*, as listed in Section 3.1 and Fig. 6).

3.3.1 Flow patterns

Flow patterns and velocity distributions of the *FBB* and in practical engineering bifurcation under working conditions *A*-*C* are shown in Fig. 8. The method described is comparable to the research by Adechy (2004) in the modeling of annular flow through pipes and *T*-junctions.

The velocity was generally well distributed in the *FBB*. Some typical flow patterns are shown in Fig. 8. The velocity decreased while the pressure value increased in the expansion sections and the velocity increased while the pressure value decreased in the contraction sections. Accompanied by flow separation and backflow, the velocity increased and the pressure decreased near the convex corners. The velocity of the main stream decreased, and regional flow separation was observed behind the rib, while the back flow was not obvious.

Flow patterns in the *FBB* were quite similar to those in the *CRB*, but the local flow patterns were slightly different in the entrance of the branch pipe. The waist turning angle of the main and cone pipes was greater than for the *CRB* with a transition pipe, so the maximum velocity was greater than for the *CRB* under working conditions *A*, *B*, and *C*.

In working condition *C*, the main streams came from the two branch pipes which impacted each other near the rib. In working condition *B*, the streamline bent with decreasing velocity were more evident than in other working conditions. Thus, the shape of the *FBB* did not degrade the flow regime. On the contrary, the *FBB* was superior to the others under the two pump working conditions.

3.3.2 Head loss

The long-term economic benefits of a hydropower station are directly affected by the head loss in bifurcations. It affects the feasibility of this new shape directly. We list the head loss coefficients of the FBB and the practical engineering bifurcation in Table 2, using the results under each working condition mentioned above.

Compared with the *CRB*, the head loss for the *FBB* was slightly greater, but within an acceptable range. This was primarily caused by the non-horizontal cone pipe axis. Thus, the main streams were separated after the crotch, and then deflected downward in the cone pipe. The

Table 2 Head loss coefficients of the FBB and the practical engineering bifurcation under each working condition

Type of bifurcation	Working condition *A*		Working condition *B*		Working condition *C*	
	K_{31}	K_{32}	K_{31}	K_{32}	K_{13}	K_{23}
The *FBB*	0.337	0.337	0.721	——	0.418	0.419
The *CRB*	0.312	0.313	0.645	——	0.405	0.406

streamline was bent more evidently and generated greater energy losses. The head loss coefficients were 0.025, 0.076, and 0.013 larger than in the *CRB* under working conditions *A*, *B*, and *C*, respectively. This clearly showed that the condition with two turbines working was preferable to that with one turbine working. Flow patterns were better distributed when two pumps were working, which proved to be very feasible for pumped storage power stations.

3.4 Economic efficiency

3.4.1 Steel consumption

With regard to manufacturing and installation, the new *Y*-typed *FBB* has a concise shape design, and there are no transitional sections, compared with the *CRB*, so it has fewer pipe sections and a more regular shape.

Based on the computational models, the steel consumption for the *FBB* was 54 428.3 kg, while that for the *CRB* was 67 144.8 kg. Although it has waist girders, the steel consumption for this part was only 202.3 kg. Therefore, the *FBB* decreased the steel consumption by about 18% compared with the *CRB*.

3.4.2 Excavation volume

Owing to the waist girders of the bifurcations in hydropower stations, construction is generally difficult, with regard to underground transportation and welding. However, the rib is a part of the *U*-shaped reinforced girder in the *FBB*. It was confirmed that it reduced the extensive width of reinforced girders from the *FEM* analysis in previous sections. Compared with the *CRB*, it slightly decreased the excavated section and excavation volume. Thus, this new shape is also suitable for embedded steel bifurcations.

4. Conclusions

Bifurcations play an important role in the water diversion systems in PHESs. However, there is no efficient solution to the drainage problem, and pecuniary loss always occurs upon the periodic overhaul of hydropower stations. To solve this problem, a new *Y*-typed *FBB* was designed in this study, which was shown not only to retain the advantages of commonly used bifurcations, but also enables drainage due to gravity, which markedly improved the draining time.

An applicable design philosophy was proposed in this study. All of the fundamental curves were determined, including profile curves and intersecting curves, by which the *FBB* could be uniquely shaped. Furthermore, compared with a *CRB* in practice, both the structural and the hydraulic characteristics of this new type of bifurcation were investigated, and its feasibility was demonstrated.

Structural characteristics based on *FEM* proved the practicability of the *Y*-typed *FBB*. There were no significant stress concentration areas or clear large displacements in the bifurcations. The mechanics were reasonable, and the majority of stresses were lower than those found in practice for the same pipe thickness.

The flow pattern in the *FBB* was quite analogous to that found in practice, and the shape change of the *FBB* did not degrade the flow regime. The head loss for the *FBB* was slightly greater, but still acceptable. The condition with two turbines working was clearly better than with one turbine working, and flow patterns were better distributed when the two pumps were working.

This bifurcation can decrease the steel consumption in manufacturing compared with that found for the bifurcation in practice, and it can slightly decrease the excavated section and excavation volume compared with the *CRB*. It proved effective and feasible in pumped storage power stations, and the *FBB* was also shown to be suitable for embedded steel bifurcation. Drainage due to gravity, which shortens the draining time, and its feasibility, demonstrated potential for relatively wide applications.

Acknowledgments

This paper was based on a study carried out by the authors at the State Key Laboratory of Water Resources and Hydropower Engineering Science and Changjiang River Scientific Research Institute. The authors are grateful to the National Natural Science Foundation of China for its financial support (No. 51409194).

References

Adechy, D. and Issa, R.I. (2004), "Modelling of annular flow through pipes and T-junctions", *Comput. Fluid.*, **33**(2), 289-313.

American Society of Civil Engineers (2012), ASCE Manuals and Reports on Engineering Practice No.79 *Steel Penstocks*, 2rd Edition, American Society of Mechanical Engineers.

ANSYS Inc. (2011), ANSYS FLUENT User's Guide, Version 14.0, Canonsburg, PA.

ANSYS Inc. (2011), ANSYS Structural Analysis Guide, Version 14.0, Canonsburg, PA.

Ardizzon, G., Cavazzini, G. and Pavesi, G. (2014), "A new generation of small hydro and pumped-hydro power plants: Advances and future challenges", *Renew. Sustain. Energy Rev.*, **31**, 746-761.

Austin, R.G., Waanders, B.V.B., McKenna, S. and Choi, C.Y. (2008), "Mixing at cross junctions in water distribution systems II: Experimental study", *J. Water Res. Plan. Manag.*, **134**(3), 295-302.

Bassett, M.D., Winterbone, D.E. and Pearson, R.J. (2001), "Calculation of steady flow pressure loss coefficients for pipe junctions", *Proceedings of the Institution of Mechanical Engineers, Part C: J. Mech. Eng. Sci.*, **215**(8), 861-881.

Cheng, Y.G. and Yang, J.D. (2005), "Hydraulic resistance coefficient determination of throttled surge tanks by means of computational fluid dynamics", *J. Hydra. Eng.*, **7**,787-792.

Deane, J.P., Ó Gallachóir, B.P. and McKeogh, E.J. (2010), "Techno-economic review of existing and new pumped hydro energy storage plant", *Renew. Sustain. Energy Rev.*, **14**(4), 1293-1302.

Dhatt, G., Lefrançois, E. and Touzot, G. (2012), *Finite Element Method*, John Wiley and Sons.

Ferziger, J.H. and Perić, M. (2002), *Computational Methods for Fluid Dynamics*, 3rd Edition, Springer, Berlin.

Gan, G. and Riffat, S.B. (2000), "Numerical determination of energy losses at duct junctions", *Appl. Energy*, **67**(3), 331-340.

German, V.A., Komleva, N.A. and Rytchenko, E.N. (1998), "Design and calculation of the steel penstocks and forks of the hydroelectric station at the shahid abbaspour dam", *Hydrotech. Constr.*, **32**(3), 168-170.

Hafiz, Y.A., Younan, M.Y. and Abdalla, H.F. (2012), "Limit and Shakedown loads determination for locally thinned wall pipe branch connection subjected to pressure and bending moments", *ASME 2012 Pressure Vessels and Piping Conference*, American Society of Mechanical Engineers.

Jeong, W. and Seong, J. (2014), "Comparison of effects on technical variances of computational fluid dynamics (CFD) software based on finite element and finite volume methods", *Int. J. Mech. Sci.*, **78**, 19-26.

Kim, Y.J., Lee, K.H. and Park, C.Y. (2006), "Limit loads for thin-walled piping branch junctions under

internal pressure and in-plane bending", *Int. J. Press. Ves. Pip.*, **83**(9), 645-653.
Kim, Y.J., Lee, K.H. and Park, C.Y. (2008), "Limit loads for piping branch junctions under internal pressure and in-plane bending-Extended solutions", *Int. J. Press. Ves. Pip.*, **85**(6), 360-367.
Lee, K.H., Kim, Y.J., Budden, P.J. and Nikbin, K. (2009), "Plastic limit loads for thick-walled branch junctions", *J. Strain Anal. Eng. Des.*, **44**(2), 143-148.
Lee, K.H., Xu, Y., Jeon, J.Y., Kim, Y.J. and Budden, P.J. (2012), "Plastic limit loads for piping branch junctions under out-of-plane bending", *J. Strain Anal. Eng. Des.*, **47**(1), 32-45.
Liu, H. and Li, P. (2013), "Even distribution/dividing of single-phase fluids by symmetric bifurcation of flow channels", *Int. J. Heat Fluid Flow*, **40**, 165-179.
Myeong, M.S., Kim, Y.J. and Budden, P.J. (2012), "Limit load interaction of cracked branch junctions under combined pressure and bending", *Eng. Fract. Mech.*, **86**, 1-12.
Nazari, M.E., Ardehali, M.M. and Jafari, S. (2010), "Pumped-storage unit commitment with considerations for energy demand, economics, and environmental constraints", *Energy*, **35**(10), 4092-4101.
Papatheocharis, T., Diamanti, K., Varelis, G.E., Perdikaris, P.C. and Karamanos, S.A. (2013), "Experimental and numerical investigation of pipe T-junctions under strong cyclic loading", *ASME 2013 Pressure Vessels and Piping Conference*, American Society of Mechanical Engineers.
Pérez-García, J., Sanmiguel-Rojas, E. and Viedma, A. (2009), "New experimental correlations to characterize compressible flow losses at 90-degree T-junctions", *Exper. Therm. Fluid Sci.*, **33**(2), 261-266.
Pérez-García, J., Sanmiguel-Rojas, E. and Viedma, A. (2010), "New coefficient to characterize energy losses in compressible flow at T-junctions", *Appl. Math. Model.*, **34**(12), 4289-4305.
Pérez-García, J., Sanmiguel-Rojas, E., Hernández-Grau, J. and Viedma, A. (2006), "Numerical and experimental investigations on internal compressible flow at T-type junctions", *Exper. Therm. Fluid Sci.*, **31**(1), 61-74.
Romero-Gomez, P., Ho, C.K. and Choi, C.Y. (2008), "Mixing at cross junctions in water distribution systems I: Numerical study", *J. Water Res. Plan. Manag.*, **134**(3), 285-294.
Seppälä, M. and Volcheck, E. (2012), *Computational Algebraic and Analytic Geometry*, American Mathematical Society.
Shih, T.H., Liou, W.W., Shabbir, A., Yang, Z. and Zhu, J. (1995), "A new k-ϵ eddy viscosity model for high reynolds number turbulent flows", *Comput. Fluid.*, **24**(3), 227-238.
Storozhuk, E.A., Chernyshenko, I.S. and Kharenko, S.B. (2012b), "Elastoplastic deformation of conical shells with two circular holes", *Int. Appl. Mech.*, **48**(3), 127-132.
Storozhuk, E.A., Chernyshenko, I.S. and Rudenko, I.B. (2012a), "Elastoplastic state of spherical shells with cyclically symmetric circular holes", *Int. Appl. Mech.*, **48**(5), 573-582.
Tang, J.L., Wang, L.W. and Li, X. (2009), "Resistance characteristics of hydraulic oil through isodiametric T-type duct with sharp corners", *Chin. J. Mech. Eng.*, **22**(2), 250-255.
Thomas, G.B., Finney, R.L., and Weir, M.D. (1988), *Calculus and Analytic Geometry*, Vol.7, Addison-Wesley, Reading, MA.
Ure, J., Chen, H. and Tipping, D. (2013), "Calculation of a lower bound ratchet limit part 2 - Application to a pipe intersection with dissimilar material join", *Eur. J. Mech. A/Solid.*, **37**, 369-378.
Van, D.J. and Raithby, G.D. (1984), "Enhancement of the SIMPLE method for predicting incompressible fluid flow", *Numer. Heat Transf.*, **7**(2), 147-163.
White, F.M. (2008), *Fluid Mechanic*s, 6th Edition, McGraw-Hill, New York.
Wilcox, D.C. (1993), *Turbulence Modeling for CFD*, DCW Industries, Inc., La Canada, Calif.
Xuan, F.Z. and Li, P.N. (2004), "Finite element-based limit load of piping branch junctions under combined loadings", *Nucl. Eng. Des.*, **231**(2), 141-150.
Xuan, F.Z., Li, P.N. and Tu, S.T. (2003), "Evaluation of plastic limit load of piping branch junctions subjected to out-of-plane moment loadings", *J. Strain Anal. Eng. De.*, **38**(5), 395-404.
Xuan, F.Z., Li, P.N. and Tu, S.T. (2006), "Limit load analysis for the piping branch junctions under in-plane moment", *Int. J. Mech. Sci.*, **48**(4), 460-467.
Xuan, F.Z., Liu, C.J. and Li, P.N. (2005), "An approximative solution for limit load of piping branch

junctions with circumferential crack and finite element validation", *Nucl. Eng. Des.*, **235**(7), 727-736.
Yamaguchi, F. and Yamaguchi, F. (1988), *Curves and Surfaces in Computer Aided Geometric Design*, Springer-Verlag, Berlin.
Zhang, Q.L. and Wu, H.G. (2013), "Using softened contact relationship describing compressible membrane in FEA of spiral case structure", *Arch. Civil Mech. Eng.*, **13**(4), 506-517.

CC

Abbreviations and Nomenclature

CFD	Computational fluid dynamics
CRB	Crescent-ribbed bifurcation
FBB	Flat-bottomed bifurcation
FEM	Finite element modeling
PHES	Pumped hydro energy storage plant
RGB	Reinforced girders bifurcation
L_B	Axis length of branch pipe
L_M	Axis length of main pipe
R_B	Radius of branch pipe
R_N	Radius of main pipe
W_R	Maximum width of rib
W_U	Width of *U*-shaped extension reinforced girders
W_W	Width of waist reinforced girders
α	Taper apex angle of cone pipe
φ	Horizontal projection angle of the bifurcation